

Conversely, G0s2-Flag was coimmunoprecipitated with F<sub>o</sub>F<sub>1</sub>-ATP synthase (Fig. S4C). G0s2-Flag was also found to be associated with the F<sub>o</sub>F<sub>1</sub>-ATP synthase in 293T and HeLa cells (Fig. S4C). Both coimmunoprecipitation using an anti-G0s2 antibody and a reciprocal immunoprecipitation revealed that endogenous G0s2 interacts with F<sub>o</sub>F<sub>1</sub>-ATP synthase, whereas none of the proteins in complexes I–IV or adenine nucleotide translocase 1 (ANT1; also referred to as ADP/ATP carrier) were coimmunoprecipitated with G0s2 (Fig. 4 B and C).

Given that the G0s2 protein contains an evolutionarily conserved amino terminus and one hydrophobic domain (HD) (19), we created three G0s2 partial deletion mutants to identify the domain in G0s2 that is important for binding to F<sub>o</sub>F<sub>1</sub>-ATP synthase (Fig. S4D). Among these mutants, G0s2 ΔC and G0s2 ΔN but not G0s2 ΔHD bound to the F<sub>o</sub>F<sub>1</sub>-ATP synthase complex (Fig. 4D and Fig. S4 E and F). Furthermore, we confirmed that G0s2 directly interacts with F<sub>o</sub>F<sub>1</sub>-ATP synthase in an in vitro pull-down assay using a recombinant maltose-binding protein–fused G0s2 protein and purified F<sub>o</sub>F<sub>1</sub>-ATP synthase from bovine heart mitochondria (Fig.

S5). Immunocytochemical analysis revealed that endogenous G0s2 colocalized with the β-subunit of F<sub>o</sub>F<sub>1</sub>-ATP synthase (Fig. 4E). The knockdown of G0s2 expression by shRNA abolished G0s2 staining (Figs. S6 and S7A), indicating that both antibodies used for immunostaining specifically recognize G0s2. These data suggest that G0s2 interacts with the F<sub>o</sub>F<sub>1</sub>-ATP synthase complex through its HD in mitochondria and regulates OXPHOS activity.

**G0s2 Increases Mitochondrial ATP Production Rate.** [ATP]<sub>mito</sub> is mainly determined by the rate of ATP synthesis by F<sub>o</sub>F<sub>1</sub>-ATP synthase and ATP/ADP exchange by the ATP/ADP translocase ANT1. This theory means that the increased [ATP]<sub>mito</sub> observed in the G0s2-overexpressing cells may result from the increased ATP synthesis and/or decreased ATP/ADP exchange, although G0s2 did not interact with ANT1 (Fig. 4B). To resolve this issue and directly measure the rate of ATP production in mitochondria, we used a semiintact cell system called the mitochondrial activity of streptolysin O permeabilized cells (MASC) assay (25). In this assay, we permeabilized the plasma membrane to wash out any cytosolic components, such as creatine and glycolytic substrates, but left the mitochondria intact. Furthermore, we treated the cells with P<sup>1</sup>, P<sup>5</sup>-di(adenosine-5') pentaphosphate to inhibit the activity of adenylate kinase. These steps allowed us to measure the ATP production rate mostly from OXPHOS, with a minimal contribution of ATP buffering systems in the cytosol. The MASC assay was suitable for accurate measurement of mitochondrial ATP production rate, because mitochondria in this semiintact cell system suffered much smaller damage than the isolated mitochondria in the conventional method. Surprisingly, in the MASC assay, the ATP production rate markedly increased when G0s2 was expressed in HeLa cells that lacked endogenous G0s2 (Fig. 5A). In cardiomyocytes, shRNA-mediated G0s2 knockdown decreased the ATP production rate in mitochondria, and the expression of G0s2 WT but not G0s2 ΔHD could restore the ATP production rate (Fig. 5B and Fig. S7A). In both cells, complete inhibition of ATP production by oligomycin A indicated that the observed ATP synthesis was catalyzed by OXPHOS but not other metabolism (Fig. 5 A and B).

Next, to evaluate the physiological role of G0s2, we examined whether endogenous G0s2 induced by hypoxia could enhance the ATP production rate. Cardiomyocytes were pretreated with hypoxia for 4 h, during which G0s2 expression was largely induced. We then evaluated the ATP production rate of both hypoxia-pretreated and nontreated cardiomyocytes under room air conditions. Even under these equivalent normoxic conditions, hypoxia-pretreated cardiomyocytes produced ATP faster than nontreated control cardiomyocytes (Fig. 5C and Fig. S7B). G0s2 knockdown attenuated this increase in the rate of ATP production, indicating that the enhanced ATP production rate resulting from hypoxia pretreatment primarily depends on endogenous G0s2 induction. This increased G0s2 expression was essential for cell survival, because G0s2-depleted cells died earlier than control cells under conditions of hypoxic stress (Fig. 5D).

Furthermore, to assess the effect of G0s2 on cellular respiration, we continuously measured the oxygen consumption rate (OCR) using an XF96 Extracellular Flux Analyzer. G0s2 knockdown decreased the basal OCR of cardiomyocytes, most likely because of the decreased activity of ATP synthesis (Fig. 5 E and F). In contrast, the proton leakage of the mitochondrial inner membrane and the maximum respiratory capacity of OXPHOS complexes I–IV were unaffected by G0s2 ablation (Fig. 5 E and F). These data show that G0s2 knockdown reduced respiration caused by ATP synthesis without affecting respiration caused by proton leakage, nonmitochondrial respiration, or the maximal respiration capacity.

All these findings indicate that G0s2 enhances the mitochondrial ATP production rate by increasing the activity of F<sub>o</sub>F<sub>1</sub>-ATP synthase.

## Discussion

In this study, we showed that G0s2 kinetically increased OXPHOS activity through direct binding to F<sub>o</sub>F<sub>1</sub>-ATP synthase. Our previous

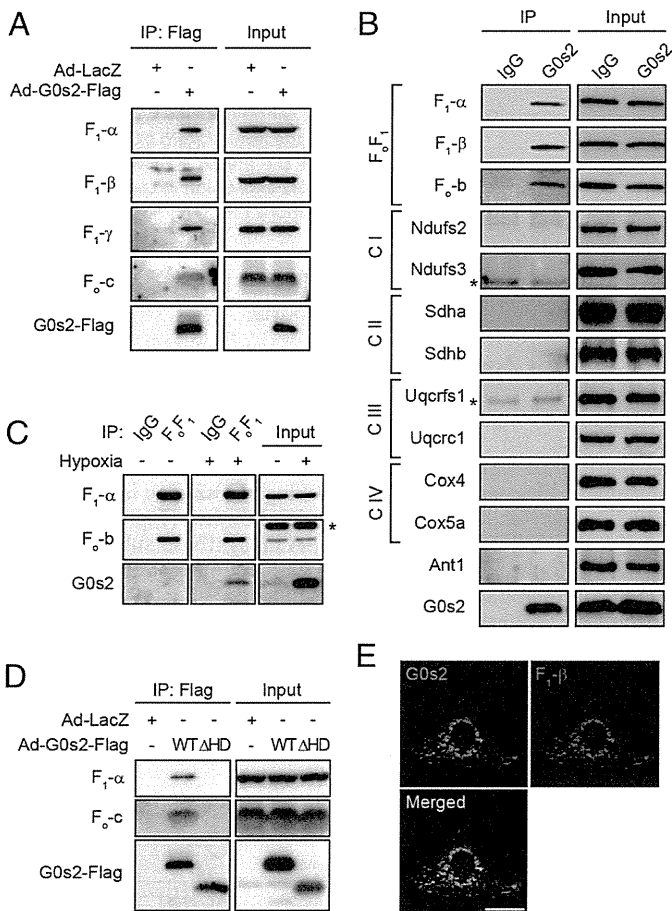


**Fig. 4.** G0s2 interacts with the F<sub>o</sub>F<sub>1</sub>-ATP synthase in mitochondria. (A) Immunoprecipitation (IP) of G0s2-Flag in cardiomyocytes. Cell lysates from cardiomyocytes expressing G0s2-Flag or LacZ were immunoprecipitated with an anti-Flag antibody. (B) IP of endogenous G0s2 in cardiomyocytes. Endogenous G0s2 was induced by hypoxia and immunoprecipitated using an anti-G0s2 antibody. C, OXPHOS complex; F<sub>o</sub>F<sub>1</sub>, F<sub>o</sub>F<sub>1</sub>-ATP synthase. \*IgG light chain. (C) IP of F<sub>o</sub>F<sub>1</sub>-ATP synthase in cardiomyocytes under normoxic or hypoxic conditions. Cell lysates from cardiomyocytes cultured under normoxia or hypoxia for 4 h were immunoprecipitated with an antibody against the whole F<sub>o</sub>F<sub>1</sub>-ATP synthase complex or a control IgG. \*Nonspecific band. (D) IP of G0s2 mutants expressed in cardiomyocytes. Cell lysates were immunoprecipitated with an anti-Flag antibody. (E) Immunostained images of hypoxia-stimulated (4 h) cardiomyocytes with anti-G0s2 (green) and anti-F<sub>o</sub>F<sub>1</sub>-ATP synthase β-subunit (red) antibodies. (Scale bars: 20 μm.)

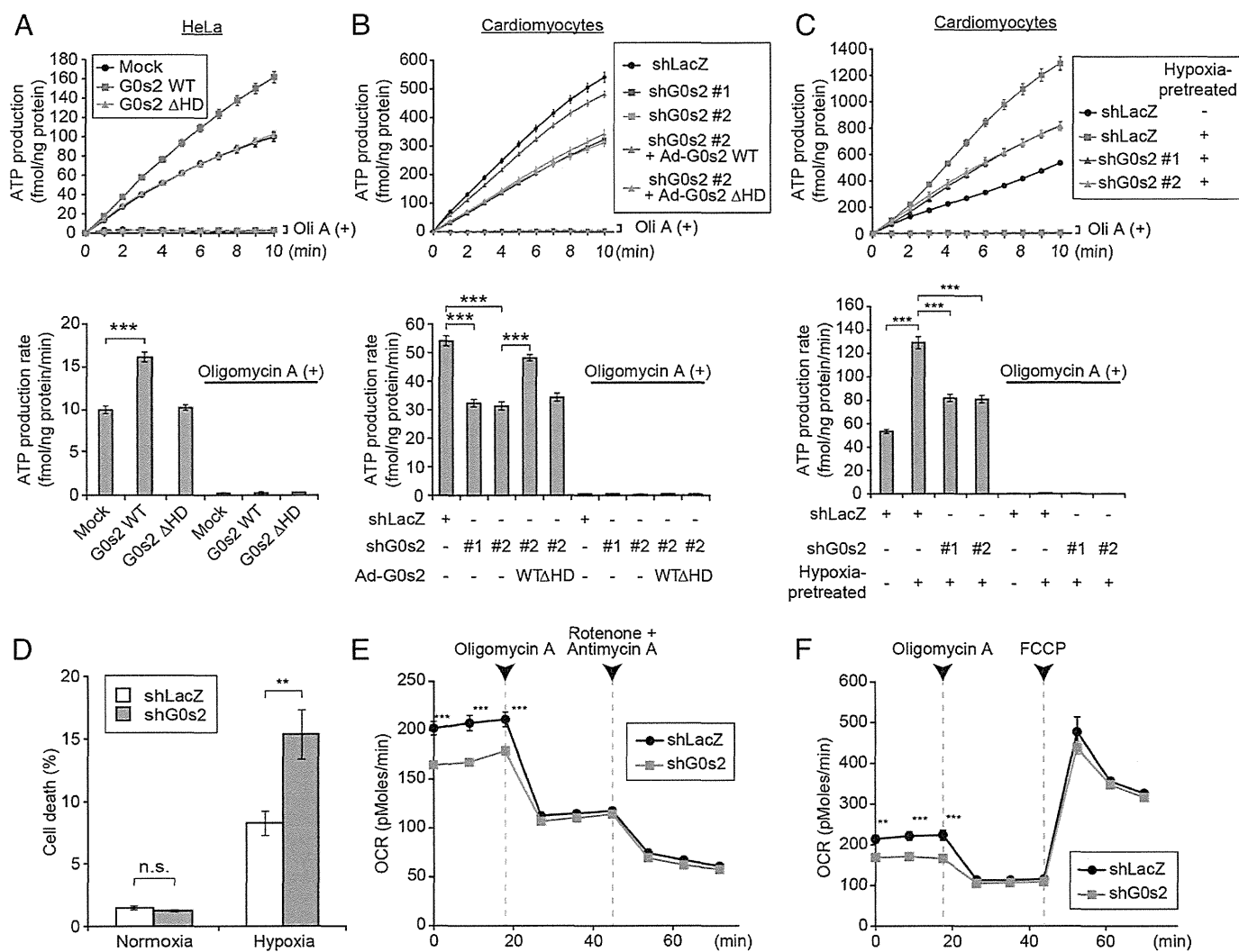


**Fig. 5.** G0s2 enhances the mitochondrial ATP production rate. (A and B) MASC assay of (A) permeabilized HeLa cells expressing the indicated plasmids or (B) cardiomyocytes expressing the indicated adenovirus in the presence (dotted lines) or absence (solid lines) of 1  $\mu$ M oligomycin A (Oli A). Upper shows the ATP production plots, and Lower shows the mean ATP production rates between 0 and 10 min. (A)  $n = 12$ . (B) Solid lines,  $n = 12$ ; dotted lines,  $n = 8$ . (C) MASC assay of permeabilized cardiomyocytes pretreated with hypoxia. Cells expressing the indicated adenovirus were pretreated with or without hypoxia for 4 h. After the pretreatment, the cells were permeabilized under room air conditions followed by MASC assay in the presence (dotted lines;  $n = 8$ ) or absence (solid lines;  $n = 12$ ) of 1  $\mu$ M Oli A. Upper shows the ATP production plot, and Lower shows the mean ATP production rate between 0 and 10 min. (D) The bar graph represents the cell viability of G0s2-depleted cardiomyocytes under hypoxic conditions. Cardiomyocytes expressing shLacZ or shG0s2 (#2) were cultured under normoxic or hypoxic conditions for 18 h. (E and F) The OCR in cardiomyocytes expressing shLacZ and shG0s2 (#2) under basal conditions and in response to the indicated mitochondrial inhibitors ( $n = 8$ ). FCCP, carbonyl cyanide-4-(trifluoromethoxy)-phenylhydrazone. Data are represented as the means  $\pm$  SEMs. n.s., not significant.  $^{**}P < 0.01$ ;  $^{***}P < 0.001$ .

studies of  $F_0F_1$ -ATP synthase have revealed that this enzyme has a specific structure that connects two molecular nanomotors that synchronize with each other to produce ATP (26–30). These physically distinct structures suggest that a specific activating factor for  $F_0F_1$ -ATP synthase must exist. Combined with the findings from this study, we hypothesize that G0s2 may lower the activation barrier of the  $F_0F_1$ -ATP synthase nanomotor and enhance the ATP production rate with the equivalent proton motive driving force (PMF; i.e., the sum of the membrane potential and the pH gradient). Activation barriers might be generated by various factors, such as friction between the stator and rotor of  $F_0F_1$ -ATP synthase, physical and electrical resistance to proton transport through the channel, and the existence of rotary blockers such as the bacterial  $\epsilon$ -subunit and cyclophilin D (31). The increased ATP production rate caused by G0s2 overexpression observed in the MASC assay supports this hypothesis, because the PMF in the initial phase of this assay should be the same. If this hypothesis is true, even with reduced PMF, cells that express G0s2 should produce ATP faster than cells that express

little or no G0s2. In fact, G0s2 overexpression attenuated the decline of  $[ATP]_{\text{mito}}$  under hypoxic conditions that reduced the PMF. Precise real-time measurement of the PMF is currently difficult, but these hypotheses might be proven in future studies. Kinetically faster ATP production should accompany greater consumption of both  $O_2$  and PMF; however, our results suggest that preserving ATP production is more beneficial than preserving PMF for cell viability, particularly when the  $O_2$  supply is restricted but still exists. The transience of endogenous G0s2 expression induced by hypoxia might serve to protect tissues in the early phase of energy crisis. There may be specific mechanisms to decrease G0s2 expression under prolonged ischemia that have yet to be identified. Another possible mechanism by which G0s2 could increase the ATP production rate is that G0s2 increases the  $F_0F_1$  coupling efficiency of  $F_0F_1$ -ATP synthase. However, this hypothesis is less likely, because G0s2 altered the oxygen consumption rate to increase the ATP production rate. Although this uncoupling phenomenon has rarely been reported for mammalian mitochondrial  $F_0F_1$ -ATP synthase, we cannot completely eliminate the possibility that intrinsically

uncoupled  $F_0F_1$ -ATP synthase exists, because we could not accurately measure the amount of uncoupled  $F_0F_1$ -ATP synthase in intact cells.

G0s2 was first identified in cultured monocytes during the drug-induced cell cycle transition from G0 to G1 phase (18, 32). A limited number of studies have implied that G0s2 is involved in cell proliferation (33), differentiation (19), apoptosis (34), inflammation (35), and lipid metabolism (36) in various cellular settings. Moreover, G0s2 was reported to localize to the cytosol (33), endoplasmic reticulum (19), mitochondria (34), or the surface of lipid droplets (36). How G0s2 distinguishes these multiple functions is still not clear. In our hands, G0s2 is always localized to mitochondria, which was shown by immunostaining with two antibodies against different epitopes of G0s2 (Fig. S6). Complete depletion of mitochondrial staining by G0s2 knockdown strongly suggests the specific localization of G0s2 to mitochondria. We also showed that G0s2 specifically bound to mitochondrial  $F_0F_1$ -ATP synthase but not other OXPHOS protein complexes and functionally regulated OXPHOS activity. Together, these data suggest that G0s2 acts in the mitochondria. However, different cellular conditions may change the localization and role of G0s2. Additionally, G0s2-mediated changes in ATP metabolism may possibly affect the lipid metabolism or cellular proliferation. Additional studies will reveal the functional mechanisms by which G0s2 exerts these multiple functions in different cellular conditions.

In this study, we evaluated  $[ATP]_{mito}$  and  $[ATP]_{cyto}$  separately using FRET-based ATP biosensors in living cells. This dual evaluation revealed that  $[ATP]_{mito}$  reflected mitochondrial ATP production with much greater sensitivity than  $[ATP]_{cyto}$  (Fig. 1 and Movies S1 and S2). Because  $[ATP]_{cyto}$  is strongly influenced by the activity of various cytosolic ATP hydrolytic enzymes and

ATP buffering enzymes,  $[ATP]_{cyto}$  does not always reflect the ATP availability that determines cellular function.

Taken together, our results indicate that G0s2 is a positive regulator of OXPHOS that works to increase the mitochondrial ATP production rate even under hypoxic conditions. Therefore, enhancing the level and function of G0s2 could be beneficial for hypoxia- and mitochondria-related disorders, such as ischemic diseases, metabolic diseases, and cancer.

## Materials and Methods

Cells were infected with adenovirus encoding FRET-based ATP indicators AT1.03 or mit-AT1.03 to measure changes in cytosolic or mitochondrial ATP concentrations, respectively. Image acquisitions and FRET analyses were performed as described previously with some modifications (13). For the control of oxygen concentration during time-lapse imaging, digital gas mixer for stage-top incubator GM8000 (Tokai Hit) was used to create hypoxic (1%  $O_2$ ) or normoxic (20%  $O_2$ ) condition. Additional methods are found in *SI Materials and Methods*.

**ACKNOWLEDGMENTS.** We thank M. Murata for helpful discussions and advice, H. Miyagi (Olympus Co. Ltd.) for technical advice regarding microscopy, T. Miyazaki (Cyclax Co. Ltd.) for making antibodies, S. Ikezawa and A. Ogai for technical assistance, K. Tanaka for help with the purification of bovine  $F_0F_1$ -ATP synthase, and Y. Okada and H. Fujii for secretarial support. This research was supported by the Japan Society for the Promotion of Science through the Funding Program for Next Generation World-Leading Researchers (NEXT Program) initiated by the Council for Science and Technology Policy; grants-in-aid from the Ministry of Health, Labor, and Welfare-Japan; and grants-in-aid from the Ministry of Education, Culture, Sports, Science, and Technology-Japan. This research was also supported by grants from Takeda Science Foundation, Japan Heart Foundation, Japan Cardiovascular Research Foundation, Japan Intractable Diseases Research Foundation, Japan Foundation of Applied Enzymology, Japan Medical Association, Uehara Memorial Foundation, Mochida Memorial Foundation, Banyu Foundation, Naito Foundation, Inoue Foundation for Science, Osaka Medical Research foundation for Intractable Diseases, Ichiro Kanehara Foundation, and Showa Houkokuai.

- Kim JW, Tchernyshov I, Semenza GL, Dang CV (2006) HIF-1-mediated expression of pyruvate dehydrogenase kinase: A metabolic switch required for cellular adaptation to hypoxia. *Cell Metab* 3(3):177–185.
- Papandreou I, Cairns RA, Fontana L, Lim AL, Denko NC (2006) HIF-1 mediates adaptation to hypoxia by actively downregulating mitochondrial oxygen consumption. *Cell Metab* 3(3):187–197.
- Semenza GL (2012) Hypoxia-inducible factors in physiology and medicine. *Cell* 148(3):399–408.
- Semenza GL, et al. (1996) Hypoxia response elements in the aldolase A, enolase 1, and lactate dehydrogenase A gene promoters contain essential binding sites for hypoxia-inducible factor 1. *J Biol Chem* 271(51):32529–32537.
- Chen YC, et al. (2012) Identification of a protein mediating respiratory supercomplex stability. *Cell Metab* 15(3):348–360.
- Fukuda R, et al. (2007) HIF-1 regulates cytochrome oxidase subunits to optimize efficiency of respiration in hypoxic cells. *Cell* 129(1):111–122.
- Strogolova V, Furness A, Robb-McGrath M, Garlich J, Stuart RA (2012) Rcf1 and Rcf2, members of the hypoxia-induced gene 1 protein family, are critical components of the mitochondrial cytochrome bc1-cytochrome c oxidase supercomplex. *Mol Cell Biol* 32(8):1363–1373.
- Saks V, et al. (2006) Cardiac system bioenergetics: Metabolic basis of the Frank-Starling law. *J Physiol* 571(Pt 2):253–273.
- Smolenski RT, Lachno DR, Ledingham SJ, Yacoub MH (1990) Determination of sixteen nucleotides, nucleosides and bases using high-performance liquid chromatography and its application to the study of purine metabolism in hearts for transplantation. *J Chromatogr A* 527(2):414–420.
- Shimura D, et al. (2013) Metabolomic profiling analysis reveals chamber-dependent metabolite patterns in the mouse heart. *Am J Physiol Heart Circ Physiol* 305(4):H494–H505.
- Kemp GJ, Meyerspeer M, Moser E (2007) Absolute quantification of phosphorus metabolite concentrations in human muscle in vivo by 31P MRS: A quantitative review. *NMR Biomed* 20(6):555–565.
- Ford SR, et al. (1996) Use of firefly luciferase for ATP measurement: Other nucleotides enhance turnover. *J Biolumin Chemilumin* 11(3):149–167.
- Imamura H, et al. (2009) Visualization of ATP levels inside single living cells with fluorescence resonance energy transfer-based genetically encoded indicators. *Proc Natl Acad Sci USA* 106(37):15651–15656.
- Lopaschuk GD, Kelly DP (2008) Signalling in cardiac metabolism. *Cardiovasc Res* 79(2):205–207.
- Hattori F, et al. (2010) Nongenetic method for purifying stem cell-derived cardiomyocytes. *Nat Methods* 7(1):61–66.
- Forsythe JA, et al. (1996) Activation of vascular endothelial growth factor gene transcription by hypoxia-inducible factor 1. *Mol Cell Biol* 16(9):4604–4613.
- Wolf A, et al. (2011) Hexokinase 2 is a key mediator of aerobic glycolysis and promotes tumor growth in human glioblastoma multiforme. *J Exp Med* 208(2):313–326.
- Russell L, Forsdyke DR (1991) A human putative lymphocyte G0/G1 switch gene containing a CpG-rich island encodes a small basic protein with the potential to be phosphorylated. *DNA Cell Biol* 10(8):581–591.
- Zandbergen F, et al. (2005) The G0/G1 switch gene 2 is a novel PPAR target gene. *Biochem J* 392(Pt 2):313–324.
- Heckmann BL, Zhang X, Xie X, Liu J (2013) The G0/G1 switch gene 2 (G0S2): Regulating metabolism and beyond. *Biochim Biophys Acta* 1831(2):276–281.
- Dimroth P, von Ballmoos C, Meier T (2006) Catalytic and mechanical cycles in F-ATP synthases. Fourth in the Cycles Review Series. *EMBO Rep* 7(3):276–282.
- Senior AE (2007) ATP synthase: Motoring to the finish line. *Cell* 130(2):220–221.
- Walker JE (1998) ATP synthesis by rotary catalysis (Nobel Lecture). *Angew Chem Int Ed* 37:5000–5011.
- Yoshida M, Muneyuki E, Hisabori T (2001) ATP synthase—a marvellous rotary engine of the cell. *Nat Rev Mol Cell Biol* 2(9):669–677.
- Fujikawa M, Yoshida M (2010) A sensitive, simple assay of mitochondrial ATP synthesis of cultured mammalian cells suitable for high-throughput analysis. *Biochem Biophys Res Commun* 401(4):538–543.
- Adachi K, et al. (2007) Coupling of rotation and catalysis in F(1)-ATPase revealed by single-molecule imaging and manipulation. *Cell* 130(2):309–321.
- Itoh H, et al. (2004) Mechanically driven ATP synthesis by F1-ATPase. *Nature* 427(6973):465–468.
- Noji H, Yasuda R, Yoshida M, Kinoshita K, Jr. (1997) Direct observation of the rotation of F1-ATPase. *Nature* 386(6622):299–302.
- Rondelez Y, et al. (2005) Highly coupled ATP synthesis by F1-ATPase single molecules. *Nature* 433(7027):773–777.
- Uchihashi T, Iino R, Ando T, Noji H (2011) High-speed atomic force microscopy reveals rotary catalysis of rotorless F<sub>1</sub>-ATPase. *Science* 333(6043):755–758.
- Giorgio V, et al. (2009) Cyclophilin D modulates mitochondrial F0F1-ATP synthase by interacting with the lateral stalk of the complex. *J Biol Chem* 284(49):33982–33988.
- Siderovski DP, Blum S, Forsdyke RE, Forsdyke DR (1990) A set of human putative lymphocyte G0/G1 switch genes includes genes homologous to rodent cytokine and zinc finger protein-encoding genes. *DNA Cell Biol* 9(8):579–587.
- Yamada T, Park CS, Burns A, Nakada D, Lacorazza HD (2012) The cytosolic protein G0S2 maintains quiescence in hematopoietic stem cells. *PLoS ONE* 7(5):e38280.
- Welch C, et al. (2009) Identification of a protein, G0S2, that lacks Bcl-2 homology domains and interacts with and antagonizes Bcl-2. *Cancer Res* 69(17):6782–6789.
- Kobayashi S, et al. (2008) Expression profiling of PBMC-based diagnostic gene markers isolated from vasculitis patients. *DNA Res* 15(4):253–265.
- Yang X, et al. (2010) The G(0)/G(1) switch gene 2 regulates adipose lipolysis through association with adipose triglyceride lipase. *Cell Metab* 11(3):194–205.

# Liposomal Amiodarone Augments Anti-arrhythmic Effects and Reduces Hemodynamic Adverse Effects in an Ischemia/Reperfusion Rat Model

Hiroyuki Takahama · Hirokazu Shigematsu · Tomohiro Asai · Takashi Matsuzaki · Shoji Sanada · Hai Ying Fu · Keiji Okuda · Masaki Yamato · Hiroshi Asanuma · Yoshihiro Asano · Masanori Asakura · Naoto Oku · Issei Komuro · Masafumi Kitakaze · Tetsuo Minamino

Published online: 24 January 2013  
© Springer Science+Business Media New York 2013

## Abstract

**Purpose** Although amiodarone is recognized as the most effective anti-arrhythmic drug available, it has negative hemodynamic effects. Nano-sized liposomes can accumulate in and selectively deliver drugs to ischemic/reperfused (I/R) myocardium, which may augment drug effects and reduce side effects. We investigated the effects of liposomal amiodarone on lethal arrhythmias and hemodynamic parameters in an ischemia/reperfusion rat model.

**Methods and Results** We prepared liposomal amiodarone (mean diameter:  $113 \pm 8$  nm) by a thin-film method. The left coronary artery of experimental rats was occluded for 5 min followed by reperfusion. Ex vivo fluorescent imaging revealed

that intravenously administered fluorescent-labeled nano-sized beads accumulated in the I/R myocardium. Amiodarone was measurable in samples from the I/R myocardium when liposomal amiodarone, but not amiodarone, was administered. Although the intravenous administration of amiodarone (3 mg/kg) or liposomal amiodarone (3 mg/kg) reduced heart rate and systolic blood pressure compared with saline, the decrease in heart rate or systolic blood pressure caused by liposomal amiodarone was smaller compared with a corresponding dose of free amiodarone. The intravenous administration of liposomal amiodarone (3 mg/kg), but not free amiodarone (3 mg/kg), 5 min before ischemia showed a significantly reduced duration of lethal arrhythmias ( $18 \pm 9$  s) and mortality (0 %) during the reperfusion period compared with saline ( $195 \pm 42$  s, 71 %, respectively).

**Conclusions** Targeting the delivery of liposomal amiodarone to ischemic/reperfused myocardium reduces the mortality due to lethal arrhythmia and the negative hemodynamic changes caused by amiodarone. Nano-size liposomes may be a promising drug delivery system for targeting I/R myocardium with cardioprotective agents.

T. Matsuzaki · S. Sanada · H. Y. Fu · K. Okuda · M. Yamato · Y. Asano · I. Komuro · T. Minamino (✉)  
Department of Cardiovascular Medicine, Osaka University Graduate School of Medicine, 2-2 Yamadaoka, Suita, Osaka 565-0871, Japan  
e-mail: minamino@cardiology.med.osaka-u.ac.jp

H. Takahama · M. Asakura · M. Kitakaze  
Department of Cardiovascular Medicine, National Cerebral and Cardiovascular Center, Suita 565-8565, Japan

H. Shigematsu · T. Asai · N. Oku  
Department of Medical Biochemistry and Global COE, University of Shizuoka Graduate School of Pharmaceutical Sciences, Shizuoka 422-8526 Shizuoka, Japan

H. Asanuma  
Department of Cardiovascular Science and Technology, Kyoto Prefectural University School of Medicine, Kyoto 602-8566, Japan

H. Takahama  
Division of Cardiovascular Disease, Mayo Clinic, Rochester, MN 55902, USA

**Keywords** Liposome · Amiodarone · Lethal arrhythmia · Ischemia · Reperfusion

## Introduction

Therapies for the prevention and treatment of ischemia-induced life-threatening arrhythmias remain an unmet medical need [1]. Amiodarone is currently considered to be the most effective anti-arrhythmic drug available for treating life-threatening arrhythmias [2, 3], despite the fact that this compound has a negative impact on hemodynamic parameters [4, 5]. The intravenous administration of amiodarone is expected

to be beneficial for the immediate treatment of arrhythmias in emergency settings, such as acute myocardial infarction (AMI) [6, 7]. However, in clinical practice, the administration of amiodarone remains problematic for the treatment of AMI [8]. Although lower doses of amiodarone result in fewer incidences of death, high doses of amiodarone can cause hypotension and non-cardiac death, both of which may diminish the positive effects of amiodarone [8, 9]. Therefore, a novel delivery system is strongly desired to enhance the anti-arrhythmic effects of amiodarone without producing severe side effects.

Liposomes are widely used for drug delivery to actively or passively target specific organs and to improve drug stability in cancer and inflammatory diseases [10–12]. In ischemic/reperfused (I/R) myocardium, cellular permeability is enhanced and vascular endothelial integrity is disrupted [13, 14], suggesting that nanoparticles, such as liposomes, may be a promising drug delivery system for targeting I/R myocardium with cardioprotective agents [15]. Indeed, we have recently demonstrated that adenosine encapsulated by liposomes coated with polyethylene glycol (PEG) exhibited enhanced cardioprotective effects and attenuated side effects, such as hypotension and bradycardia, in an ischemia/reperfusion model of rats [16]. In the present study, we prepared liposomal amiodarone and examined 1) the targeted accumulation of liposomal amiodarone in the I/R myocardium, 2) the hemodynamic effects of the intravenous administration of liposomal amiodarone and free amiodarone, and 3) the anti-arrhythmic effects of these preparations in an I/R rat model. We showed that targeting the delivery of liposomal amiodarone to I/R myocardium reduces the mortality due to lethal arrhythmias and the negative hemodynamic changes caused by amiodarone in an I/R rat model.

## Methods

### Materials

The materials used to prepare PEGylated liposomes, including 1-palmitoyl-2-oleoyl-sn-glycero-3-phosphocholine (POPC), 1,2-dipalmitoyl-sn-glycero-3-phosphocholine (DPPC), cholesterol, and 1,2-distearoyl-sn-glycero-3-phosphoethanolamine-N-poly(ethylene glycol) 2000 (DSPE-PEG2000), were kindly donated by Nippon Fine Chemical Co. (Taka-sago, Hyogo, Japan). Fluorescent beads (diameter 100 nm) were purchased from Invitrogen. All other materials were obtained from Sigma-Aldrich (St. Louis, MO, USA).

### Animals

Male Wistar rats (9 weeks old and weighing 250–310 g; Japan Animals, Osaka, Japan) were used. The animal experiments were approved by the Osaka University Research Committee

and were performed according to institutional guidelines. All studies conformed to the Guide for the care and Use of Laboratory Animals published by the US National Institutes of Health (NIH Publication No. 85–23, revised 1996).

### Preparation of PEGylated Liposomes

PEGylated liposomes composed of POPC, DPPC, cholesterol, DSPE-PEG2000, and amiodarone were prepared by a thin-film method. Briefly, amiodarone and lipids dissolved in chloroform were evaporated to form a thin lipid film using a rotary evaporator. The lipid film was dried for at least 1 h under reduced pressure and then hydrated with PBS (pH 7.4). The liposome solution was freeze-thawed for 3 cycles with liquid nitrogen. The particle size of the liposomes was adjusted by extrusion through 100-nm-pore polycarbonate filters (Nuclepore, Cambridge, MA, USA). The liposomal solutions were centrifuged at 453,000 g for 15 min (CS120GXL, Hitachi, Japan) to remove the untrapped amiodarone. Then, the liposomes were resuspended in PBS. To determine the efficacy of trapping amiodarone in the liposomes, an aliquot of the liposomal solution was solubilized with 1 % reduced Triton X-100 (Sigma-Aldrich), and the amount of amiodarone was optically determined at 240 nm.

### Characterization of PEGylated Liposomes

The particle size and  $\zeta$  potential of PEGylated liposomes diluted with PBS were measured by dynamic scatter analysis (Zetasizer Nano ZS; Malvern, Worcestershire, UK). The analyses were performed 15 times per sample, and the results represent the analysis of 3 independent experiments.

### Experimental Protocol

#### *Targeted Delivery of Fluorescent-labeled Nano-sized Beads to the I/R Myocardium*

The rats were anesthetized with intraperitoneal sodium pentobarbital (50 mg/kg). Catheters were advanced into the femoral vein to infuse the drugs. Ischemia/reperfusion was induced by 5 min of left coronary artery occlusion followed by reperfusion [16]. After the hemodynamic parameters became stable, fluorescent-labeled nano-size beads, 100 nm in diameter (FluoSpheres, Invitrogen), were intravenously infused to the rats for 5 min before ischemia or before a sham operation ( $n=3$ , each). Fifteen minutes after reperfusion, the hearts were removed and cut into 5 sections parallel to the axis from the base to the apex. Then, ex vivo fluorescence images were obtained with an Olympus SZX12 stereoscopic microscope equipped with a DP71 digital camera (Olympus, Tokyo, Japan) before and after the hearts were sliced.

### *Targeted Delivery of Amiodarone and Liposomal Amiodarone to the I/R Myocardium*

Catheters were advanced into the femoral artery and vein to measure the systemic blood pressure (BP) and to infuse the drugs into the anesthetized rats, respectively. Electrocardiographic and hemodynamic parameters, such as heart rate (HR) and BP, were continuously monitored during the study using a PowerLab system (ADInstruments, Castle Hill, Australia). After the hemodynamic parameters became stable, to clarify the targeted delivery of amiodarone and liposomal amiodarone to the I/R myocardium, we intravenously administered saline, free amiodarone (3 mg/kg) or liposomal amiodarone (3 mg/kg) to rats for 5 min before the onset of ischemia. Then, we obtained blood samples and myocardium from the I/R area.

### *Effects of Amiodarone and Liposomal Amiodarone on Lethal Arrhythmias*

To evaluate the effects of amiodarone and liposomal amiodarone on lethal arrhythmias, we intravenously administered saline ( $n=7$ ), free amiodarone (3.0 or 10.0 mg/kg) ( $n=6$  each), PEGylated liposomes (empty liposomes) ( $n=6$ ), and PEGylated liposomal amiodarone (3.0 mg/kg) ( $n=6$ ) for 5 min before ischemia. The dose of amiodarone used in this study was lower than that used in a previous study [17] to clarify whether amiodarone encapsulated by liposomes coated with PEG exhibited enhanced anti-arrhythmic effects. Without any procedure such as electrical conversion or cardiac massage, ventricular tachyarrhythmias (VT/VF) occurred frequently during early period of reperfusion and the mortality of rats reached more than a half of cases in this model [18].

### *Measurement of Amiodarone Concentration*

The concentration of amiodarone in serum and heart tissue from the I/R area was assayed by high-performance liquid chromatography (HPLC) as previously described [19]. The detection limit of the HPLC assay was 50 ng/mL. Blood and myocardial samples were obtained at the end of the experimental protocol. The sample preparation was performed as previously described [19]. Briefly, myocardium was freed from visible blood, thereafter rinsed with 0.9 % sodium chloride and stored at  $-20\text{ }^{\circ}\text{C}$  until analysis. After that, myocardial tissue samples were finely minced and 100 mg were homogenized with 0.9 % sodium chloride (1 mL) and after centrifugation, the clear supernatant was injected into HPLC.

### *Quantitative Evaluation of Fluorescent-labeled Nano-sized Beads in the I/R Myocardium*

To analyze the quantitative fluorescent intensity, signals from heart slices were quantified by image analysis (Image

J; National Institutes of Health, USA) as previously described [20]. The signal intensity from the heart slices was evaluated as the average signals of the whole heart and the left ventricle (LV) (Fig. 2c).

### *Arrhythmia Analysis*

The electrocardiographic tracings were independently analyzed by two of the authors, who were blinded to the treatment assignment. The duration of each spontaneous ventricular tachycardia or fibrillation episode during the I/R protocol was measured using the time scale provided by the recording software. Ventricular tachycardia was defined as 4 or more consecutive ventricular ectopic beats, and ventricular fibrillation was defined as a signal in which the individual QRS deflections could not easily be distinguished from one another. However, distinguishing ventricular tachycardia from fibrillation was often difficult [21]; therefore, we report ventricular tachycardia and fibrillation collectively as ventricular tachyarrhythmias (VT/VF) in this study. VT/VF duration and mortality were evaluated for 5 min of ischemia followed by 15 min of reperfusion.

### *Statistical Analysis*

The parameters of the liposomes are expressed as the mean  $\pm$  standard deviation (SD). Other data are expressed as the average  $\pm$  standard error of the mean (SEM). To compare the parameters of the liposomes, unpaired *t*-tests were performed. We performed the Welch *t*-test to compare the amiodarone concentration in the plasma and myocardium. For hemodynamic parameters, the data were assessed with the paired *t*-test for comparisons to the baseline within a group. One-way repeated-measurement ANOVA followed by post-hoc Bonferroni's multiple comparisons were used for comparisons between groups. To address the differences in VT/VF duration among the groups, we performed a non-parametric (Kruskal-Wallis) test followed by evaluation with the Mann-Whitney *U* test. The mortality rates were compared using the Fisher's exact probability test. In all analyses,  $P<0.05$  was considered to be statistically significant.

## **Results**

### *Characterization of PEGylated Liposomes*

We prepared 5 types of PEGylated liposomes composed of POPC, DPPC, cholesterol, and amiodarone. The ratio of unsaturated lipids (POPC) to saturated lipids (DPPC) varied (Fig. 1). During preparation of the liposomes, the POPC:DPPC:cholesterol:amiodarone molar ratio of 10:0:5:1 exhibited the best encapsulation efficiency for amiodarone compared with the other conditions (Fig. 1).

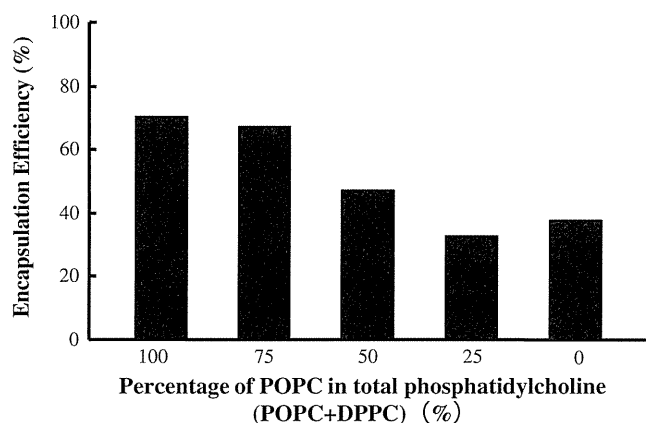


**Fig. 1** Encapsulation efficiency of amiodarone in the liposomes. Amiodarone was loaded into liposomes containing POPC, DPPC, or a mixture of POPC and DPPC. The liposomal amiodarone was composed of phosphatidylcholine (POPC + DPPC):cholesterol:amiodarone at a 10:5:1 molar ratio. The percent molar ratio of POPC in total phosphatidylcholine (POPC + DPPC) is indicated in the figure. The encapsulation efficiency of amiodarone was determined as described in the Methods section

The dynamic light scatter analysis showed no significant differences between the mean diameter, polydispersity index, or  $\zeta$  potential distribution of the empty and amiodarone-loaded PEGylated liposomes (Table 1).

#### Accumulation of Fluorescence-labeled Nano-sized Beads in the I/R Myocardium

Representative pictures obtained by fluorescence imaging are shown in Fig. 2a (whole heart) and b (sliced hearts). Quantitative analysis revealed that the average fluorescence intensity of the whole heart (Fig. 2c left) or the left ventricle (Fig. 2c right) of the I/R hearts was significantly higher than that in sham-operated hearts.

#### Amiodarone Concentration in the Blood and I/R Myocardium

The plasma concentration after the administration of liposomal amiodarone was significantly higher than that of free amiodarone (Table 2). Importantly, the amiodarone concentration in the I/R myocardium was detectable after the administration of liposomal, but not free, amiodarone (Table 2).

#### Hemodynamic Effects of Amiodarone and Liposomal Amiodarone

The baseline heart rates were  $411 \pm 16$ ,  $426 \pm 14$ ,  $427 \pm 12$ ,  $409 \pm 8$  and  $414 \pm 6$  beats/min in the saline, empty liposome, amiodarone (3 mg/kg), amiodarone (10 mg/kg) and liposomal amiodarone (3 mg/kg) groups, respectively. The baseline systolic BP was  $113 \pm 7$ ,  $118 \pm 10$ ,  $111 \pm 5$ ,  $90 \pm 4$  and  $104 \pm 2$  mmHg in the saline, empty liposome, amiodarone (3 mg/kg), amiodarone (10 mg/kg) and liposomal amiodarone (3 mg/kg) groups, respectively. There were no significant differences in the baseline HR or systolic BP among the groups tested. The intravenous administration of amiodarone (3 and 10 mg/kg) or liposomal amiodarone reduced both the HR and systolic BP from the baseline, whereas the saline or empty liposomes did not (Fig. 3). The time-course changes of both the HR and systolic BP were significantly smaller in the liposomal amiodarone group (3 mg/kg) compared with the corresponding dose in the free amiodarone group (3 mg/kg) (Fig. 3). The reductions in HR and systolic BP at 1, but not 3, minutes after liposomal amiodarone administration were significantly smaller compared with those following the corresponding dose of amiodarone.

#### Antiarrhythmic Effects of Amiodarone and Liposomal Amiodarone

Representative electrocardiograms of the rats that received saline, free amiodarone or liposomal amiodarone are shown in Fig. 4. The intravenous administration of liposomal amiodarone (3 mg/kg), but not amiodarone (3 mg/kg), significantly reduced the duration of VT/VF compared with saline (Table 3). Furthermore, the mortality in the group that received liposomal amiodarone (3 mg/kg), but not the corresponding dose of amiodarone (3 mg/kg), was significantly lower than that in the saline group. In the group of rats that received a high dose of amiodarone (10 mg/kg), the VT/VF duration was  $36 \pm 12$  s, and none of the rats died (Table 3), which was similar to the low dose of liposomal amiodarone group (3 mg/kg).

#### Discussion

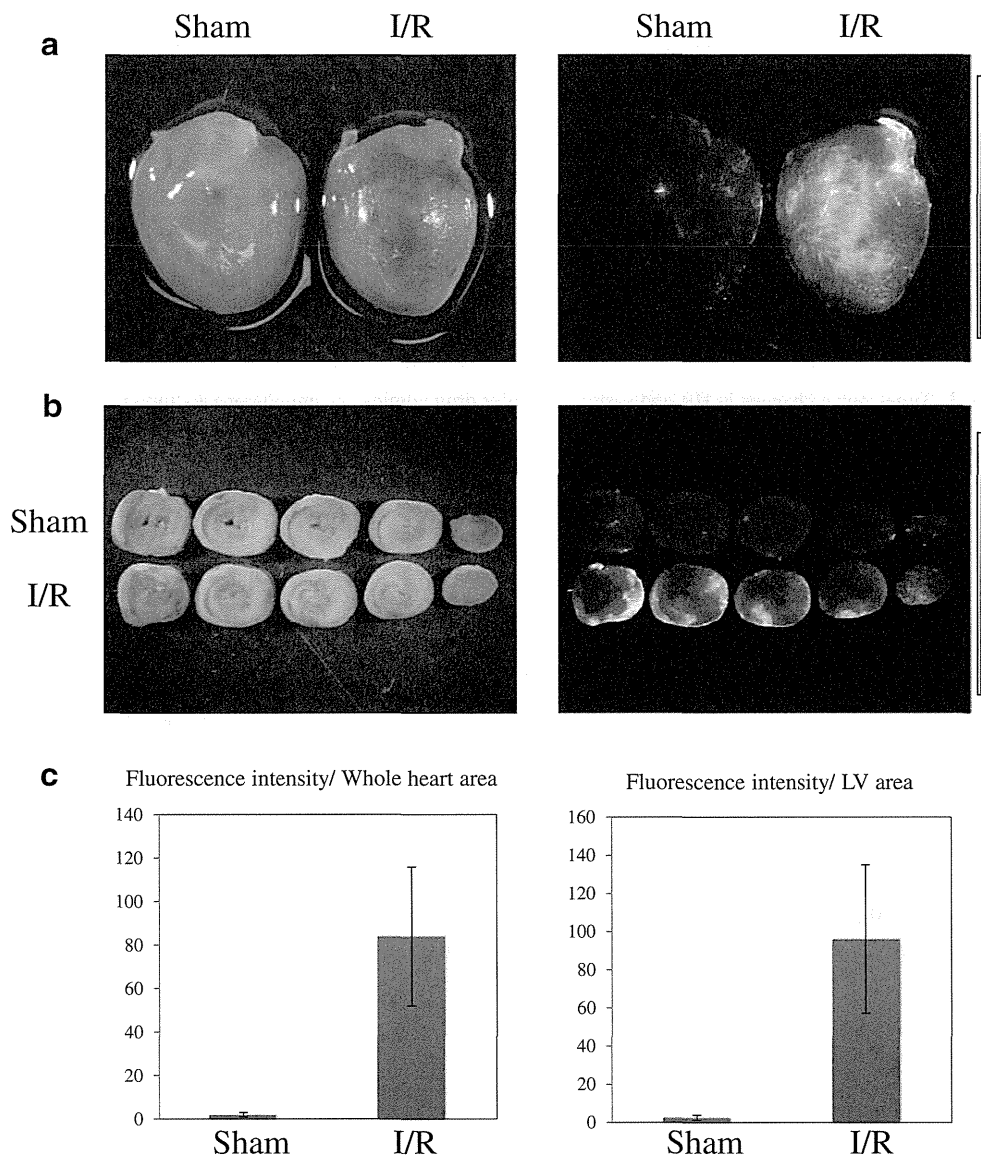
In this study, we revealed that 1) liposomal amiodarone was successfully prepared using a thin-film method, 2) the

**Table 1** Characterization of liposomes by dynamic light scatter analysis

	Mean diameter (nm)	Polydispersity index	$\zeta$ Potential (mV)
PEGylated liposomes (empty liposomes)	$111 \pm 14$	$0.124 \pm 0.027$	-2.1
PEGylated liposomal amiodarone	$113 \pm 8$	$0.128 \pm 0.040$	-3.7

Results represent 4 independent experiments. The values are expressed as the mean  $\pm$  SD. PEG polyethylene glycol

**Fig. 2** Representative pictures of ischemia/reperfused myocardium with and without fluorescence-labeled nano-sized beads. Representative pictures obtained by fluorescent imaging are shown in **a** (*whole heart*) and **b** (*sliced hearts*). Quantitative analysis revealed that the average fluorescence intensity of the whole heart (**c left**) or the left ventricle (**c right**) of the I/R hearts was significantly higher than that of the sham-operated hearts



accumulation of nano-sized beads was observed in the I/R myocardium, 3) liposomal amiodarone showed a smaller reduction in the HR and systolic BP compared with free amiodarone, and 4) liposomal amiodarone, but not amiodarone, reduced the VT/VF duration and mortality during the reperfusion period compared with saline.

**Table 2** Amiodarone concentration in the blood and I/R myocardium

Groups	Plasma, ng/mL	Myocardium, ng/mL
Saline	N.D.	N.D.
Free amiodarone	472±147	N.D.
Liposomal amiodarone	3872±378*	71±7*

Data are expressed as the mean ± SEM. N.D. not detected. n=3 rats in each group. \* p<0.05 versus free amiodarone

Preparation of Liposomal Amiodarone

This study is the first to encapsulate amiodarone in PEGylated liposomes, although it has been previously encapsulated in other liposomes [22] and micelles [23]. We demonstrated that lipid bilayers composed of unsaturated lipids are more suitable for encapsulating amiodarone in PEGylated liposomes compared with those composed of saturated lipids. PEGylated liposomes have a long circulating time in the bloodstream because PEG endows a steric barrier to liposomes, allowing them to avoid interactions with opsonins and cells of the mononuclear phagocytic system [24]. Thus, they have been used to increase drug stability, safety, and bioavailability in clinical applications. In this study, we found that a higher concentration of amiodarone was retained in the blood when we administered liposomal amiodarone compared with the administration of

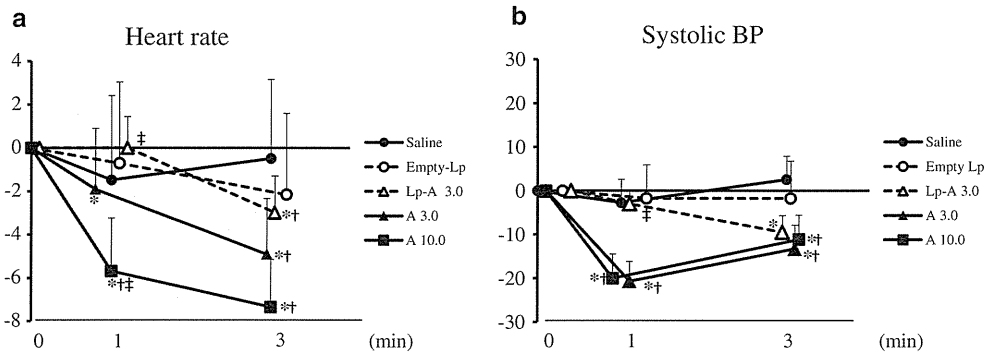


**Fig. 3** Time-course changes in HR and systolic BP after drug administration. Shows the percent change from baseline for HR (a) and systolic BP (b) after intravenous administration of the tested drugs. The data are expressed as the mean ± SEM. \* $P < 0.05$  versus baseline, paired  $t$ -test.  $P = 0.0009$  (HR),  $0.0002$  (systolic BP) between

amiodarone (3 mg/kg) and liposomal amiodarone (3 mg/kg), 1-way repeated-measurement ANOVA. † $P < 0.05$  versus saline, ‡ $P < 0.05$  versus amiodarone (3 mg/kg), 1-way repeated-measurement ANOVA with Bonferroni's multiple comparison

free amiodarone, suggesting that encapsulation of amiodarone in PEGylated liposomes enhances the stability of amiodarone in the blood.

Targeted Delivery to the I/R Myocardium by Liposomal Amiodarone

Ex vivo fluorescence imaging revealed that fluorescence-labeled nano-sized beads accumulated in the I/R myocardium, suggesting that myocardial permeability can be enhanced in the I/R myocardium. Consistent with this finding, we

observed that the amiodarone concentration in the I/R myocardium in the liposomal amiodarone group was much higher compared with that in the amiodarone group. Enhanced permeability in the I/R myocardium and the prolonged presence of amiodarone in PEGylated liposomes in the blood represent a possible mechanism for increased amiodarone concentrations in the I/R myocardium. Amiodarone will be released from accumulated liposomal amiodarone in I/R myocardium due to the natural decay and concentration gradient. These findings suggest that the I/R myocardium is a promising passive target for liposomal drug delivery.

**Fig. 4** Representative electrocardiograms. The upper, middle and lower panels show representative electrocardiograms under baseline conditions during ischemia and at the onset of reperfusion for rats that received saline, free amiodarone (3 mg/kg) and liposomal amiodarone (3 mg/kg), respectively

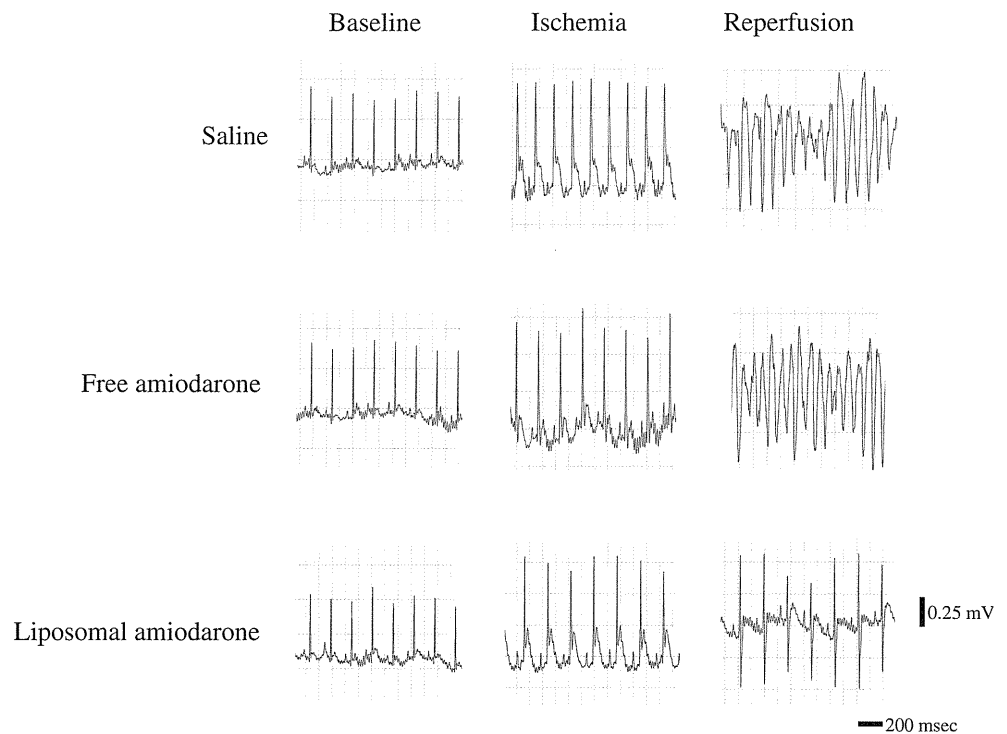


**Table 3** Lethal arrhythmias and mortality in an I/R rat model

	Number	VT/VF duration (sec)	Mortality (%)
Saline	7	195±42	71
Empty liposomes	6	162±31	50
Amiodarone (3 mg/kg)	6	167±78	33
Amiodarone (10 mg/kg)	6	36±12*	0#
Liposomal Amiodarone (3 mg/kg)	6	18±9*	0#

\* $p < 0.05$  versus saline (VT/VF duration). #  $p < 0.05$  versus saline group (mortality). VT ventricular tachycardia, VF ventricular fibrillation

#### Minimal Negative Hemodynamic Effects of Liposomal Amiodarone

Amiodarone causes hypotension and bradycardia in clinical settings [4, 5]. In this study, both free and liposomal amiodarone significantly reduced the HR and systolic BP; however, the time-course changes for both the HR and systolic BP in the liposomal amiodarone group were significantly smaller compared with those following the corresponding dose of free amiodarone. Importantly, the reductions in HR and systolic BP at 1, but not 3, minutes after liposomal amiodarone administration were significantly smaller compared with those following the corresponding dose of amiodarone. These findings suggest that liposomal amiodarone may minimize the negative effects on systemic hemodynamics immediately after the administration of amiodarone. One possible mechanism to explain this finding is that amiodarone on the surface of the liposome membrane is covered with PEG so that amiodarone cannot act directly on cardiovascular cells. Gradual release of amiodarone from liposome may minimize the rapid hemodynamic changes, because systemic hemodynamic effects of liposomal amiodarone were significantly attenuated in liposomal amiodarone group than free amiodarone group.

#### Augmented Anti-arrhythmic Effects of Liposomal Amiodarone

In this study, liposomal amiodarone (3 mg/kg), but not the corresponding dose of free amiodarone (3 mg/kg), significantly reduced the VT/VF duration and mortality compared with saline in an I/R rat model. Because the acute effects of amiodarone are known to be attributable to blockade of  $\text{Na}^+$ ,  $\text{Ca}^{2+}$  and dose-dependent  $\text{K}^+$  channels [2, 25], increasing the concentration of amiodarone in the I/R myocardium may augment its anti-arrhythmic effects through its tonic effects on cardiomyocytes caused by blocking cardiac ionic currents. Kishida et al. reported that amiodarone enhances nitric oxide production in cultured human endothelial cells [26].

Furthermore, amiodarone protects cardiac myocytes against oxidative injury by scavenging free radicals [27]. These pleiotropic effects of amiodarone are also enhanced by its increased concentration in the I/R myocardium via PEGylated liposomes, which may contribute to the reduction of lethal arrhythmias during reperfusion followed by ischemia. In the present study, since we did not do any procedure such as electrical conversion or cardiac massage for VT/VF, the mortality was higher than in our previous report [16].

#### Clinical Implications

In clinical settings, higher doses of amiodarone cause hypotension and non-cardiac death or induce worsening heart failure through negative inotropic effects [28]. These effects often diminish the beneficial effects of amiodarone for patients with AMI or heart failure [8, 9]. The present study demonstrated that liposomal amiodarone (3 mg/kg) exerts anti-arrhythmic effects similar to a high dose of free amiodarone (10 mg/kg) while reducing the extent of bradycardia and hypotension, suggesting that encapsulating amiodarone in liposomes augments its anti-arrhythmic effects and reduces its negative effects on hemodynamic parameters with reducing administrative dose. These findings can have a great impact on preventing lethal arrhythmias during reperfusion in AMI patients.

#### Study Limitations

There are several limitations in this study. We used a brief period of I/R without myocardial infarction in rats. Sakamoto et al. demonstrated that the incidence of VT/VF in a rodent model was ‘bell-shaped’ with a maximum at 5 min of ischemia and that most lethal arrhythmias occurred within first 20 s after the onset of reperfusion [29]. Consistently, our data showed that the mean time at which the lethal arrhythmia occurred after the onset of reperfusion was  $3.3 \pm 1.6$  s. Therefore, we chose the 5 min of ischemia followed by 15 min of reperfusion model. We also chose the timing of drug administration before the onset of ischemia to clarify whether liposomal-amiodarone could prevent the lethal arrhythmia that occurs in the early period of reperfusion. In addition, in clinical practice lethal arrhythmias often occur after a brief period of I/R without any irreversible damage to the heart, indicating that the anti-arrhythmic effects of liposomal amiodarone during a brief period of ischemia model could have clinical relevance [30]. However, careful interpretation is necessary when using liposomal amiodarone in acute myocardial infarction with irreversible damage to confirm the beneficial effects of liposomal amiodarone. Furthermore, because the electrophysiology of rats differs from that of humans and drug administration in our study started before the onset of

ischemia, additional pre-clinical studies including a longer period of I/R model to consider the timing of drug administration are needed using large animal models. We should also take into account that the potential side effects of amiodarone such as bradycardia are minimal in the left coronary artery occlusion model used in the present study.

## Conclusion

In conclusion, the targeted delivery of liposomal amiodarone to the I/R myocardium exerted strong anti-arrhythmic effects and reduced the negative impact on systemic hemodynamics. Nano-sized liposomes may be a promising drug delivery system for targeting the I/R myocardium with cardioprotective agents.

**Acknowledgments** The authors thank Takaki Hayakawa for her technical assistance, Takeshi Aiba for his special advice about data analysis. This research was supported by Grants-in-Aid from the Ministry of Health, Labor, and Welfare of Japan; Grants-in-Aid from the Ministry of Education, Culture, Sports, Science, and Technology of Japan; grants from the Japan Heart Foundation; and grants from the Japan Cardiovascular Research Foundation.

## References

- Di Diego JM, Antzelevitch C. Ischemic ventricular arrhythmias: experimental models and their clinical relevance. *Hear Rhythm*. 2011;8:1963–8.
- Kodama I, Kamiya K, Toyama J. Cellular electropharmacology of amiodarone. *Cardiovasc Res*. 1997;35:13–29.
- Vassallo P, Trohman RG. Prescribing amiodarone: an evidence-based review of clinical indications. *JAMA*. 2007;298:1312–22.
- Scheinman MM, Levine JH, Cannom DS, et al. Dose-ranging study of intravenous amiodarone in patients life-threatening ventricular tachyarrhythmias. The Intravenous Amiodarone Multicenter Investigators Group. *Circulation*. 1995;92:3264–72.
- Podrid PJ. Amiodarone; reevaluation of an old drug. *Ann Intern Med*. 1995;122:689–700.
- Shiga T, Tanaka T, Irie S, Hagiwara N, Kasanuki H. Pharmacokinetics of intravenous amiodarone and its electrocardiographic effects on healthy Japanese subjects. *Hear Vessel*. 2011;26:274–81.
- Wenzel V, Russo SG, Arntz HR, et al. [Comments on the 2010 guidelines on cardiopulmonary resuscitation of the European Resuscitation Council.]. *Anaesthesist*. 2010.
- Elizari MV, Martínez JM, Belziti C, et al. Morbidity and mortality following early administration of amiodarone in acute myocardial infarction. GEMICA study investigators, GEMA Group, Buenos Aires, Argentina. *Grupo de Estudios Multicentricos en Argentina*. *Eur Heart J*. 2000;21:198–205.
- Hu K, Gaudron P, Ertl G. Effects of high- and low-dose amiodarone on mortality, left ventricular remodeling, and hemodynamics in rats with experimental myocardial infarction. *J Cardiovasc Pharmacol*. 2004;44:627–30.
- Semalty A, Semalty M, Rawat BS, Singh D, Rawat MS. Pharmacosomes: the lipid-based new drug delivery system. *Expert Opin Drug Deliv*. 2009;6:599–612.
- Whitehead KA, Langer R, Anderson DG. Knocking down barriers: advances in siRNA delivery. *Nat Rev Drug Discov*. 2009;8:129–38.
- Malam Y, Loizidou M, Seifalian AM. Liposomes and nanoparticles: nanosized vehicles for drug delivery in cancer. *Trends Pharmacol Sci*. 2009;30:592–9.
- Horwitz LD, Kaufman D, Keller MW, Kong Y. Time course of coronary endothelial healing after injury due to ischemia and reperfusion. *Circulation*. 1994;90:2439–47.
- Dauber IM, VanBenthuyzen KM, McMurtry IF, et al. Functional coronary microvascular injury evident as increased permeability due to brief ischemia and reperfusion. *Circ Res*. 1990;66:986–98.
- Galagudza MM, Korolev DV, Sonin DL, et al. Targeted drug delivery into reversibly injured myocardium with silica nanoparticles: surface functionalization, natural biodistribution, and acute toxicity. *Int J Nanomedicine*. 2010;5:231–7.
- Takahama H, Minamino T, Asanuma H, et al. Prolonged targeting of ischemic/reperfused myocardium by liposomal adenosine augments cardioprotection in rats. *J Am Coll Cardiol*. 2009;53:709–17.
- Riva E, Hearse DJ. Anti-arrhythmic effects of amiodarone and desethylamiodarone on malignant ventricular arrhythmias arising as a consequence of ischaemia and reperfusion in the anaesthetised rat. *Cardiovasc Res*. 1989;23:331–9.
- Canyon SJ, Dobson GP. Protection against ventricular arrhythmias and cardiac death using adenosine and lidocaine during regional ischemia in the in vivo rat. *Am J Physiol Heart Circ Physiol*. 2004;287:H1286–95.
- Plomp TA, Wiersinga WM, Maes RA. Tissue distribution of amiodarone and desethylamiodarone in rats after repeated oral administration of various amiodarone dosages. *Arzneimittelforschung*. 1985;35:1805–10.
- Feige JN, Sage D, Wahli W, Desvergne B, Gelman L. PixFRET, an ImageJ plug-in for FRET calculation that can accommodate variations in spectral bleed-throughs. *Microsc Res Tech*. 2005;68:51–8.
- Opitz CF, Mitchell GF, Pfeffer MA, Pfeffer JM. Arrhythmias and death after coronary artery occlusion in the rat. Continuous telemetric ECG monitoring in conscious, untethered rats. *Circulation*. 1995;92:253–61.
- Klibanov AL, Maruyama K, Torchilin VP, Huang L. Amphipathic polyethyleneglycols effectively prolong the circulation time of liposomes. *FEBS Lett*. 1990;268:235–7.
- Theodossiou TA, Galanou MC, Paleos CM. Novel amiodarone-doxorubicin cocktail liposomes enhance doxorubicin retention and cytotoxicity in DU145 human prostate carcinoma cells. *J Med Chem*. 2008;51:6067–74.
- Elhasi S, Astaneh R, Lavasanifar A. Solubilization of an amphiphilic drug by poly(ethylene oxide)-block-poly(ester) micelles. *Eur J Pharm Biopharm*. 2007;65:406–13.
- Kamiya K, Nishiyama A, Yasui K, Hojo M, Sanguinetti MC, Kodama I. Short- and long-term effects of amiodarone on the two components of cardiac delayed rectifier K(+) current. *Circulation*. 2001;9:1317–24.
- Kishida S, Nakajima T, Ma J, et al. Amiodarone and N-desethylamiodarone enhance endothelial nitric oxide production in human endothelial cells. *Int Heart J*. 2006;47:85–93.
- Ide T, Tsutsui H, Kinugawa S, Utsumi H, Takeshita A. Amiodarone protects cardiac myocytes against oxidative injury by its free radical scavenging action. *Circulation*. 1999;100:690–2.
- Freedman MD, Somberg JC. Pharmacology and pharmacokinetics of amiodarone. *J Clin Pharmacol*. 1991;31:1061–9.
- Sakamoto J, Miura T, Tsuchida A, Fukuma T, Hasegawa T, Shimamoto K. Reperfusion arrhythmias in the murine heart: their characteristics and alteration after ischemic preconditioning. *Basic Res Cardiol*. 1999;94:489–95.
- Tzivoni D, Keren A, Granot H, Gottlieb S, Benhorin J, Stern S. Ventricular fibrillation caused by myocardial reperfusion in Prinzmetal's angina. *Am Heart J*. 1983;105:323–5.

